Chen Xi (Orcid ID: 0000-0002-0323-6532)
Li Ning (Orcid ID: 0000-0003-4178-5054)
Liu Jiawei (Orcid ID: 0000-0002-1001-3572)
Liu Yuan (Orcid ID: 0000-0002-6326-1270)

# Changes in global and regional characteristics of heat stress waves in the 21st century

**Xi Chen[1,2], Ning Li,[1,2], Jiawei Liu[3], Zhengtao Zhang[4], Yuan Liu[1,2], and Chengfang Huang[1,2]**

[1] Key Laboratory of Environmental Change and Natural Disaster, MOE, Faculty of Geographical Science, Beijing Normal University, Beijing, China
[2] Academy of Disaster Reduction and Emergency Management, Ministry of Emergency Management & Ministry of Education, Faculty of Geographical Science, Beijing Normal University, Beijing, China

[3] Collaborative Innovation Center on Forecast and Evaluation of Meteorological Disasters (CIC-FEMD)/Key Laboratory of Meteorological Disasters, Ministry of Education (KLME)/Joint International Research Laboratory of Climate and Environment Change (ILCEC), Nanjing University of Information Science and Technology, Nanjing, China
[4] Institute of Geographical Sciences and Natural Resources Research, Chinese Academy of Sciences, Beijing, China

Corresponding authors: Ning Li (ningli@bnu.edu.cn) and Jiawei Liu (liu_jiawei@foxmail.com)

**Key Points:**

- Heat stress waves are anticipated to be more intense, persistent, frequent, and influential due to anthropogenic influence.
- With the exception of maximum intensity, there is considerable regional variation in the increase of heat stress waves.
- Varying rates and trajectories at which regional heat stress waves change are independent of forcing pathway.

This article has been accepted for publication and undergone full peer review but has not been through the copyediting, typesetting, pagination and proofreading process which may lead to differences between this version and the Version of Record. Please cite this article as doi: 10.1029/2020EF001636

**Abstract**

Wet bulb globe temperature (WBGT), a combined measure of temperature and humidity effects on thermal comfort, is used to define heat stress waves (HSWs). While emerging research have raised concerns on future changes in heat stress, for the first time, this study examines spatio-temporal changes in multiple HSW characteristics (intensity, duration, frequency and cumulative mean intensity) in the 21st century under three emissions scenarios. It is the sustained nature of HSWs that impose more adverse impacts than extreme heat on a single day. HSWs are expected to be more intense, persistent, frequent, and influential due to anthropogenic influence. Models project the largest increases in multiple HSW characteristics will occur over the tropics and subtropics. The exception is maximum intensity, which displays a relative uniform increase over most global land areas. Analysis of regional population exposure to HSWs under different climate and socioeconomic scenarios emphasizes the importance of aggressive mitigation to minimize the potential impacts of HSWs. We further investigate how different regional HSW characteristics are projected to change relative to increasing global mean surface temperature (GMST). Our results confirm the varying rates and different trajectories at which regional HSWs change, independent of forcing pathway, strongly related to GMST. On both globally-aggregated and regional scales, the maximum intensity and GMST are highly linearly associated, with an approximately 1:1 increase. However, the other three HSW characteristics are projected to change at a non-linear rate per degree of GMST increase in general, and display large regional variation in the rates of their changes.

**Plain Language Summary**

Besides air temperature, air humidity is another important factor in determining the impact of heatwaves on humans. High humidity will reduce the efficiency of evaporative cooling and, when combined with high temperature, could pose a serious threat to human health or even life safety. Heat stress indexes, taking into account both temperature and humidity effects, are considered to be better indicators of environmental conditions conducive to heat stress on human health. We here employ a widely-used heat stress index, wet bulb globe temperature, to define heatwaves, namely, heat stress waves (HSWs). Heatwaves can be considered through a number of characteristics and it is their distinctive characteristics that result in the vast array of adverse impacts. This also applies to HSWs. Our results show that more intense, longer lasting, frequent, and influential HSWs are anticipated during the 21st century, and anthropogenic warming substantially increases the occurrence of HSWs. Except intensity, tropical regions will generally witness the largest increases in multiple HSW characteristics and the number of people that may be exposed to HSWs. Changes in HSW characteristics are confirmed not to depend on whether a particular warming is reached sooner or later, they strongly related to global mean surface temperature.

## 1 Introduction

A changing climate has led to increases in both mean and extreme temperatures globally since the 1950s, driven largely by anthropogenic greenhouse gas (GHG) emissions (IPCC, 2014). Research on heatwaves (warm temperature extremes) is of central importance, because they exert disproportionate impacts on societies and ecosystems compared to mean climate (e.g., Larcom et al., 2019; Mora et al., 2017; Yuan et al., 2016). More intense, frequent and longer

lasting heatwaves are projected in a future warmer climate (Fischer & Schar, 2010; Meehl & Tebaldi, 2004; Russo et al., 2014), consistent with the trend of the past decades in observations (Alexander et al., 2006).

When record-breaking heatwaves have claimed thousands of lives in recent years (Barriopedro et al., 2011; García-Herrera et al., 2010; Vogel et al., 2019), we are reminded that humans are exposed to a higher risk of heat extremes under global warming (Patz et al., 2005). Note that consideration of surface humidity is as important as that of surface temperature in defining heatwaves, since they are both directly related to body heat exchange (Basu & Samet 2002; Buzan & Huber, 2020; Kovats & Hajat, 2008; Matthews, 2018). High humidity will reduce the efficiency of evaporative cooling (that is, the main process by which the human body dissipates heat), and when combined with high air temperature, could pose a serious threat to human health or even life safety. It is therefore the combination of air temperature and humidity that really matters in indicating environmental conditions conducive to heat stress on human health (Sherwood & Huber, 2010).

Taking both temperature and humidity into consideration, some studies have reported observed increases in heat stress (Jacobs et al., 2013; Knutson & Ploshay, 2016; Raymond et al., 2020; Schoof et al., 2015; Willet & Sherwood, 2012). Recently, emerging research have raised concerns on increasing heat stress over the 21st century. Some of them indicated that heat stress will have widespread increases in mean or extreme values (Im et al., 2017; Kang & Eltahir, 2018; Matthews et al., 2017; Pal & Eltahir, 2016). More studies had greater focus on the frequency with which potentially dangerous thresholds may be exceeded (Fischer et al., 2012; Matthews et al., 2017; Mora et al., 2017; Willet & Sherwood, 2012; Zhao et al., 2015), suggesting that the tropics and sub-tropics will witness the largest increases in the threshold exceedances. There have been some research detecting the anthropogenic influence on extreme heat stress (Li et al., 2017) or assessing the related societal impacts (Coffel et al., 2018; Dunne et al., 2013).

However, it cannot be assumed that those reported increases are directly and comprehensively indicative of changes in heatwaves taking account of both temperature and humidity effects (hereafter denoted as heat stress waves). Heatwaves are broadly defined as a period of consecutive days where conditions are abnormally and uncomfortably hot, and thus can be considered through a number of characteristics, such as intensity, frequency and duration (Perkins-Kirkpatrick & Gibson, 2017). This also applies to heat stress waves (HSWs). In addition, regional analysis is much in need, because climate impacts are quite unequal in different regions (Harrington et al., 2018). Political decisions and climate agreements, like the Paris Agreement, are now more determined based on regional impacts. Since single feature of HSWs cannot deliver detailed information on them, an explicit investigation on how different HSW characteristics will change in the 21st century on both global and regional scales is warranted, yet is currently lacking in the existing literature.

To our best knowledge, the present study is the first analysis examining spatio-temporal changes in multiple characteristics of HSWs for the global level as well as regions under low, moderate, and high emissions scenarios (Representative Concentration Pathways, RCPs, 2.6, 4.5, and 8.5, respectively). Wet bulb globe temperature (WBGT), one of the most widely used heat stress index, is utilized to define HSWs and quantify their annual maximum intensity,

duration, total days, and cumulative mean intensity in this study. The probability ratio and the fraction of attributable risk are also calculated to detect changes in the probability of HSWs and the fraction attributable to humans, respectively. Finally, we analyze the potential impact of HSWs by quantifying the regional population exposure, and evaluate projected changes in HSWs as a function of global mean surface temperature (GMST). Daily outputs from climate models participating in the Coupled Model Intercomparison Project phase 5 (CMIP5) are employed and results are considered for the global land area and 26 land-based regions.

## 2 Data and Methods

### 2.1 Data

We use daily climate projections of near-surface air temperature and relative humidity from 14 CMIP5 models (Table S1). The first ensemble member (r1i1p1) of each model is utilized. Daily data for the last decades (20 to 100 years) of the pre-industrial control simulations are used to calculate HSW thresholds. The length of the control simulation analysed depends on the accessibility of both temperature and relative humidity outputs. We analyse daily output of historical simulations for the period 1986-2005 as well as future projections forced with RCP 2.6, 4.5 and 8.5 for the period 2006-2100. RCP2.6, 4.5 and 8.5, which represent 2.6 $W/m^2$, 4.5 $W/m^2$ and 8.5 $W/m^2$ of radiative forcing values in the year 2100 relative to pre-industrial values, are considered a low, moderate and high GHG concentration scenario, respectively (van Vuuren et al., 2011). Hourly near-surface air temperature and dewpoint temperature from the ERA5 reanalysis dataset during the historical period are also used to evaluate the models' performances in reproducing HSWs. All datasets from observations and models are interpolated to $0.5° \times 0.5°$ grid using a bilinear function first.

We use spatially explicit global population and gross domestic product (GDP) scenarios consistent with the Shared Socioeconomic Pathways (SSP) developed by Murakami and Yamagata (2019). The SSPs describe plausible alternative trends in the evolution of societies and ecosystems over the 21st century under the assumption of no climate change, impact, and policies (O'Neill et al., 2014). The narratives behind these scenarios have been quantified and served as common basis across climate impact, vulnerability, adaption, and mitigation research (Riahi et al., 2017). This gridded dataset includes population counts and gross productivities by 0.5 degree grids by 10 years under SSP1-SSP3. SSP1 envisions a society with low population growth and rapid social and economic development, whereas SSP3 corresponds to a society with low income growth and relatively high population growth rates in the currently high fertility countries (Jones & O'Neill, 2016). SSP2 describes a world assuming that demographic outcomes are consistent with middle of the road expectations about population growth and spatial patterns of development (Jones & O'Neill, 2016).

### 2.2 Wet Bulb Globe Temperature

In this study, WBGT is applied as the heat stress indicator. Among the various heat stress indices (Buzan et al., 2015), WBGT is the ISO standard for quantifying human thermal comfort (ISO, 1989). A direct relationship between WBGT thresholds and levels of physical activity has been demonstrated, and thus WBGT is widely adopted to develop health guidelines related to military training, outside working and sports (Willett & Sherwood, 2012). However, it requires non-standard input variables – a black globe temperature measured inside a 150 mm

diameter black globe and a wet bulb temperature measured with a wetted thermometer exposed to the wind and heat radiation. Given the difficulty to obtain black globe temperature (Lemke & Kjellstrom, 2012), we here use the 'simplified WBGT' which depends only on temperature and humidity (ABOM, 2010), following several previous studies (Chen et al., 2019; Fischer & Knutti, 2013; Lee & Min, 2018; Willett & Sherwood, 2012; Zhao et al., 2015). This 'simplified WBGT' represents heat stress for average daytime conditions outdoors (Willett & Sherwood, 2012), neglecting the effects of wind and solar insolation.

### 2.3 HSW Characteristics

We identify a HSW event when the daily WBGT exceeds its local 99th percentile (all days of year, that is, a one-in-a-hundred-days event) for at least 3 consecutive days. The percentiles are calculated at each grid point from daily data for the last decades (20 to 100 years) of the pre-industrial control simulations. The usage of a percentile-based threshold does not depend the underlying probability distribution of WBGT, allowing the quantification of HSWs across different locations. For each HSW, we quantify the following characteristics: the maximum intensity (in °C; maximum WBGT anomaly relative to the percentile threshold over the duration of the HSW), duration (in days; number of days of percentile threshold exceedance), and cumulative mean intensity (in °C day; the mean intensity multiplied by the duration of the event; Frolicher et al., 2018). The cumulative mean intensity can represent the integrated impact of a HSW on a person's health to some extent, including the effects of intensity and duration. We then calculate annual statistics, including the annual maximum intensity, the annual mean duration, the total number of HSW days per year, and the annual cumulative mean intensity. Note that the maximum intensity and duration refer to the properties of a contiguous event, so the maximum intensity does not always align with the hottest annual day. However, the total HSW days and cumulative mean intensity are independent of how they are distributed across different events in a year. Note that all globally-aggregated estimates in this paper are calculated with an area-weighted average across all global land grid points.

### 2.4 Attribution

Here, we use two metrics, probability ratio (PR) and fraction of attributable risk (FAR), to detect anthropogenic contributions to global occurrence of HSWs (Fischer & Knutti, 2015; Stott et al., 2004). Probability ratio is defined as $\mathrm{PR} = P_1/P_0$, where $P_1$ is the probability of exceeding a certain threshold in any given period (for example, the historical or future period) and $P_0$ is the probability of exceeding that threshold during the pre-industrial control period or ERA5 climatological period (that is, 0.01 for the 99th percentile). The fraction of attributable risk is then defined as $\mathrm{FAR} = 1 - (P_0/P_1) = 1 - 1/PR$. For a given HSW, its PR can be interpreted as a ratio of the occurrence of WBGT anomalies exceeding a certain local threshold. The metric FAR is better at representing a fraction of the probability of a particular HSW attributed to external influence. We extend the FAR framework to the global scale (Angélil et al., 2014; Fischer & Knutti, 2015; Frolicher et al., 2018; King et al., 2016) to determine how many fractions of HSWs occurring are attributable to human influence. Note that 'fraction of HSWs' throughout the text should be interpreted as an anthropogenic contribution to the

probability of HSWs, rather than some HSWs being anthropogenic and some not (Fischer & Knutti, 2015).To calculate a global estimate of PR, we first calculate the frequency of exceeding the 99th percentile at each land grid point in each year from 1986 to 2100. We then calculate an area-weighted average across all land grid points to estimate a global PR—and based on that a global FAR.

### 2.5 Population exposure

Exposure here is defined as the population exposed to HSWs and is calculated by multiplying population by the annual total number of HSW days in each grid (Jones et al., 2015). As such, exposure is expressed in person-days. In addition, GDP per capita is GDP divided by population at each grid point and used to account for regional vulnerability to climate change (King & Harrington, 2018). Following previous studies (Dong et al., 2015; Liu et al., 2017; Wang et al., 2016), we pair RCP2.6 with SSP1, RCP4.5 with SSP2, and RCP8.5 with SSP3. The combination of RCP2.6 and SSP1 represents the most sustainable future projection. By contrast, the combination of RCP8.5 and SSP3, represents the worst projected climatic and socioeconomic conditions. For the combination of RCP4.5 and SSP2, it reflects an intermediate pathway between RCP2.6-SSP1 and RCP8.5-SSP3.

### 2.6 Climatological biases

To access the effect of climatological biases in CMIP5 models, we apply the bias correction procedure proposed in many studies (Im et al., 2017; Kang & Eltahir, 2018; Mora et al., 2017; Pal & Eltahir, 2015). The ERA5 reanalysis data are used for the bias correction, and this methodology allows the correction of daily WBGT. Firstly, near-surface outputs from the ERA5 reanalysis dataset and each CMIP5 model are used to calculate daily WBGT during 1986-2005. Then we compute their consistent climatologies of WBGT for every global cell for any given day of the year. For each model, the magnitude of the bias for each day of the year is estimated by the difference between 30-day running means of the two climatologies. This daily bias is finally applied to the daily WBGT for the given cell and time of the year for the given model. We also calculate the HSW threshold and characteristics for each model with raw and bias-corrected data. The corresponding results from the used 14 CMIP5 models are averaged to create multi-model averages.

## 3 Results

### 3.1 Global terrestrial HSW changes

We evaluate CMIP5 model skills in terms of HSW threshold and characteristics first (Figure 1). The baseline is temporally set as the historical period (1986-2005). We determine the 99th percentile threshold of WBGT to identify HSWs in the ERA5 reanalysis data and CMIP5 historical simulations. Generally, the CMIP5 multi-model simulation reproduces the observed spatial pattern of HSW characteristics reasonably well and the latitudinal average biases are close to zero with small fluctuations (Figure 1), giving us confidence in the corresponding projections. Yet, the threshold, the number of annual total HSW days over northern Africa and the cumulative mean intensity are less well captured by the CMIP5 models (Figure 1c,l,o). We here avoid the problem of observational uncertainty, and reduce the sensitivity to model biases by calculating the percentile threshold and the corresponding characteristics of each model.

Results of multi-model mean HSW threshold and characteristics for each model with raw and bias-corrected data are displayed in Figure S1, showing a relatively high similarity between the two sources of data in general. It is probably because the use of a multi-model mean can even up biases among models (Mora et al., 2017), especially for the analyses combining temperature and humidity (Fischer & Knutti, 2013). The utility of multi-model ensemble approach gives us confidence in both global and regional projections of WBGT and different HSW characteristics. Note that the baseline for HSW threshold is then altered to the pre-industrial level, when we detect changes in different HSW characteristics in both historical (1986-2005) and future (2006-2100) simulations.

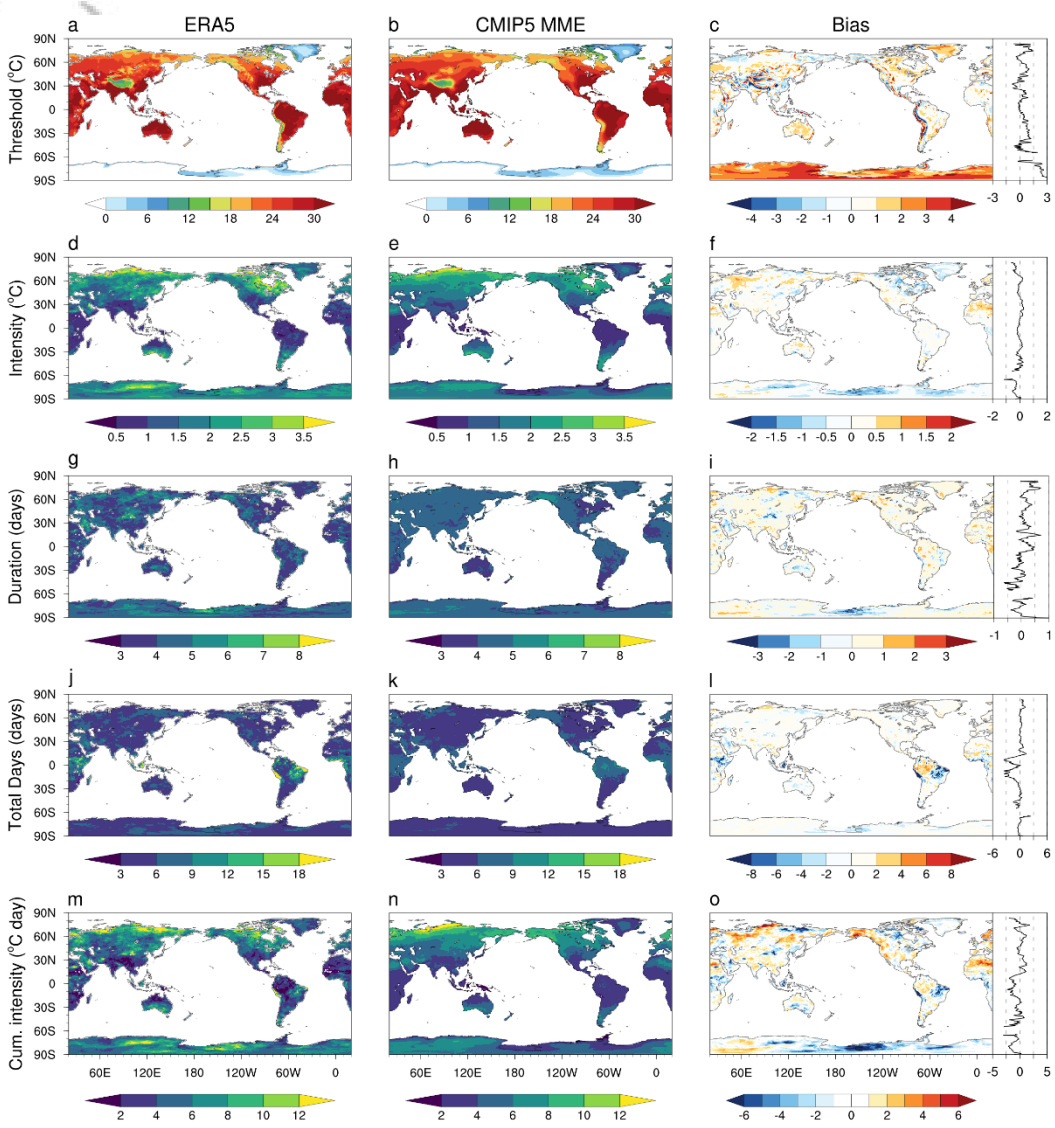


**Figure 1**. Observed (ERA5 reanalysis) and simulated (CMIP5 multi-model ensemble) global HSW characteristics and their differences (CMIP5 MME minus ERA5) averaged over the historical period (1986-2005). The threshold is set as the 99th percentile of daily WBGT in the historical period. (a), (b), (c) The 99th percentile of daily WBGT. (d), (e), (f) Maximum annual intensity of HSWs. (g), (h), (i) Annual mean duration of HSWs. (j), (k), (l) Number of annual total HSW days. (m), (n), (o) Annual cumulative mean intensity of HSWs. The curve of each rightmost graph represents zonal mean bias.

Figure 2 displays time series in global mean HSW characteristics, PR and FAR throughout the 21st century. Under RCP2.6, all HSW characteristics display very small changes. However, for the RCP 4.5 and RCP8.5 scenarios, we can see obvious increases in these characteristics. Note that all characteristics continuously increase under RCP8.5 but gradually stabilizes after the 2060s under RCP4.5. The CMIP5 models suggest that on average over global land, a HSW (with reference to preindustrial climatology) currently last 6 days, has an intensity of up to 2.1 °C and a cumulative mean intensity of 27 °C days. The number of total HSW days occurring in a year is about 27 days. By the end of the 21st century, the projected maximum intensity, duration, total days, and cumulative mean intensity will rise to around 3.8 °C, 15 days, 73 days and 121 °C days under RCP4.5, and 6.4 °C, 34 days, 115 days, and 362 °C days with the RCP8.5 simulation, respectively. Under RCP8.5, uncertainties among the CMIP5 models in the maximum intensity, duration and cumulative mean intensity become larger when projection time extends (Figure 2a,b,d). Among them, duration shows the largest multi-model spread (Figure 2b). On the contrary, the rise of total HSW days shows better consistency among the models by the end of the century (Figure 2c).

At the beginning of simulation under three emissions scenarios, the probability of 1-in-100-day HSWs over land is already about 7 times higher than in preindustrial conditions (Figure 2e). Correspondingly, the simulated FAR—that is, the anthropogenic contribution to the probability of a HSW—reaches about 0.58 (Figure 2f). This implies that roughly 58% of these extremes occurring worldwide are attributed to warming. By 2100, the simulated occurrence of extreme heat days is 12, 20 and 32 times higher than in preindustrial times under RCP2.6, RCP4.5 and RCP8.5, respectively (Figure 2e). In other words, a one-in-a-hundred-days event at preindustrial levels is projected to become a one-in-nine-days, one-in-five-days and one-in-three-days event, respectively. Results project that approximately 71%, 81% and 92% of the HSWs worldwide can be attributable to global warming with the three forcing pathways (Figure 2f).

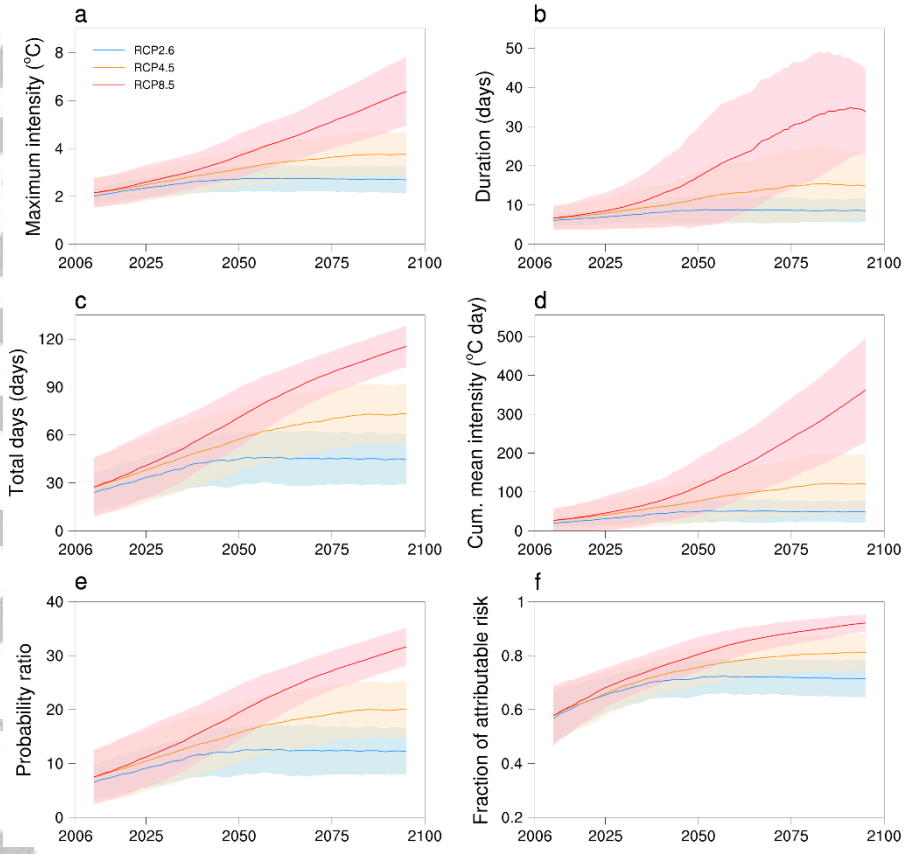


**Figure 2**. Global terrestrial changes in HSW characteristics from future simulations (2006-2100) under RCP2.6, 4.5 and 8.5. Shown are the global aggregated annual maximum intensity (a), annual mean duration (b), number of total HSW days per year (c), annual cumulative mean intensity (d), probability ratio (e), and fraction of attributable risk (f). The thick lines denote multi-model mean change, and the shaded areas indicate one multi-model standard deviation. An 11-year running mean is applied.

Under all three scenarios, the increases in maximum intensity are expected to be spatially uniform with the main exceptions of Antarctica and Greenland (Figure 3a-c). The other three characteristics all exhibit zonal differences, increasing from mid-latitudes to the equator (Figure 3d-l). Even under the most aggressive mitigation scenario (that is, RCP 2.6), people in the tropics will be exposed to HSWs for over 120 days a year more than the present-day level. The increase of total HSW days will exceed 180 days and 300 days following the RCP4.5 and RCP8.5 scenario. Moreover, the CMIP5 models project a hundred-fold increase in the annual mean duration within equatorial regions under RCP8.5. The large increase in the intensity and duration also leads to a strong increase in the cumulative mean intensity of over 900 °C days there. Still, the mid-latitudes have about 5 days, 30 days, and 100 °C days growth in terms of the duration, total HSW days and cumulative mean intensity under RCP8.5.

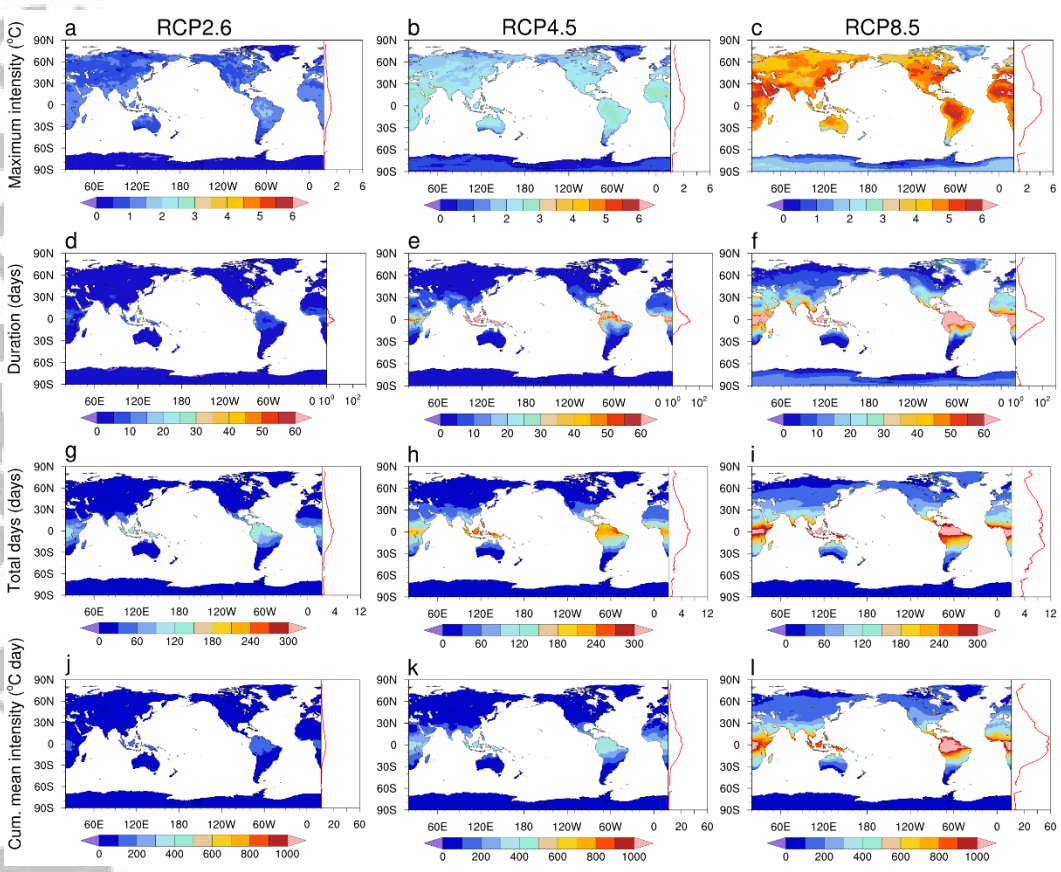


**Figure 3**. Multi-model mean changes in HSWs over the period of 2081-2100 relative to the historic baseline period (1986-2005) under alternative emission scenarios. Spatial patterns are changes in maximum annual intensity (a-c), annual mean duration (d-f), number of annual total HSW days (g-i), and cumulative mean intensity (j-l). The curve to the right of each panel represents the ratio of zonal mean variation in each HSW characteristic to its latitudinal average over the historic period. Note that we use the logarithmic scale for the curve in (d-f).

In the historical period, the climate simulations suggest an increase in the probability of HSWs relative to pre-industrial times, resulting in PR larger than 1 over global land regions (Figure 4a). Similar to the probability change of high-temperature extremes (Fischer & Knutti, 2015), the PR pattern of HSWs also features an apparent tropical peak (Figure 4a,c,e,g), resulting in the FAR of HSWs decreases from the tropics to the middle and high latitudes (Figure 4b,d,f,h). Between 1986 and 2005, the largest latitudinal average occurrence of HSWs is roughly 10 times higher than in pre-industrial conditions (Figure 4a). By the end of the century, models project it could increase by a factor of 45, 72 and 96 under RCP2.6, RCP4.5 and RCP8.5, respectively (Figure 4c,e,g). This corresponds to the largest zonal mean FAR estimate of 0.98 under RCP2.6, and its maximum value 0.99 ($1 - P_0$) under RCP4.5 and 8.5 (Figure 4d,f,h).

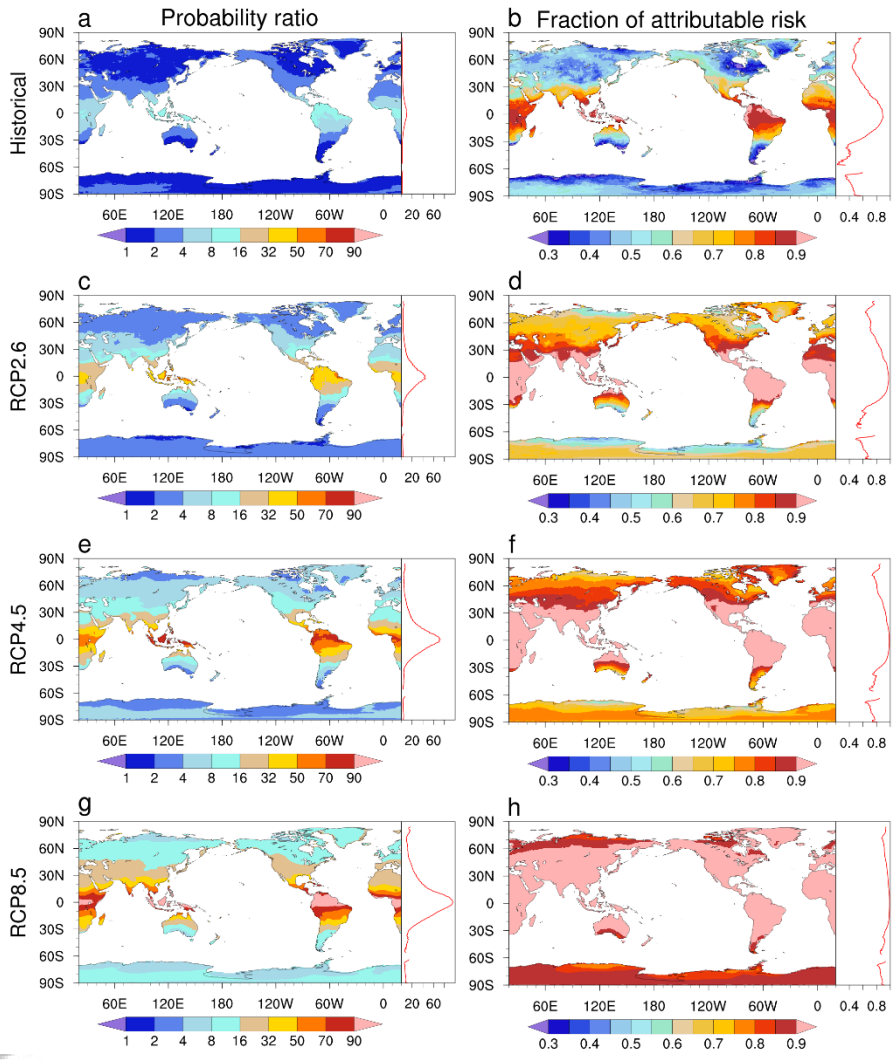


**Figure 4**. Attribution of HSWs in the historical and future periods under all three emissions scenarios. Spatial patterns are multi-model mean probability of HSW days exceeding the preindustrial 99th percentile (a,c,e,g), and anthropogenic contribution to the probability of HSWs (b,d,f,h). Distribution results are shown for the historical 1986-2005 period (a-b) and the future 2081-2100 period (c-h). The curve to the right represents latitudinal average.

### 3.2 HSW changes over world regions

While more intense, frequent and longer lasting HSWs are expected in global land areas in the future simulation, they have considerable regional variations (Figure 3). Thus we divide global land-mass between 66°S and 66°N into 26 regions (IPCC, 2012; Schleussner et al., 2016, see Figure S2 and Table S2 for details) for analysing regional changes in HSWs under all three scenarios.

The maximum intensity shows small regional variation, with an increase of about 1 °C, 1-2 °C and 4 °C (that is, multi-model medians) for all the 26 regions under RCP2.6, 4.5 and 8.5, respectively (Figure 5a-c). However, the other three characteristics differ greatly across different regions, and the largest differences emerge following the RCP8.5 scenario (Figure 5d-l). The median increase in the annual mean duration, total HSW days and cumulative mean intensity vary largely from several days to more than 100 days, from about 28 days to more

than 200 days, and from about 60 °C days to more than 600 °C days. Note that with the exception of maximum intensity, low latitude regions display the greatest differences between models, and the multi-model spread is generally reduced outside the low latitudes, indicating that higher model agreement on the HSW changes increases over these areas. This is consistent with the result reported by Perkins-Kirkpatrick and Gibson (2017) on regional changes in heatwave characteristics. Based on the increases in multiple HSW characteristics, regions of East and West Africa (EAF and WAF), Southeast Asia (SEA), Amazon (AMZ), Northeast Brazil (NEB), Central America and Caribbean (CAM), and West coast of South America (WSA) are suggested to face the most severe challenges of heat stress extremes at the end of the century.

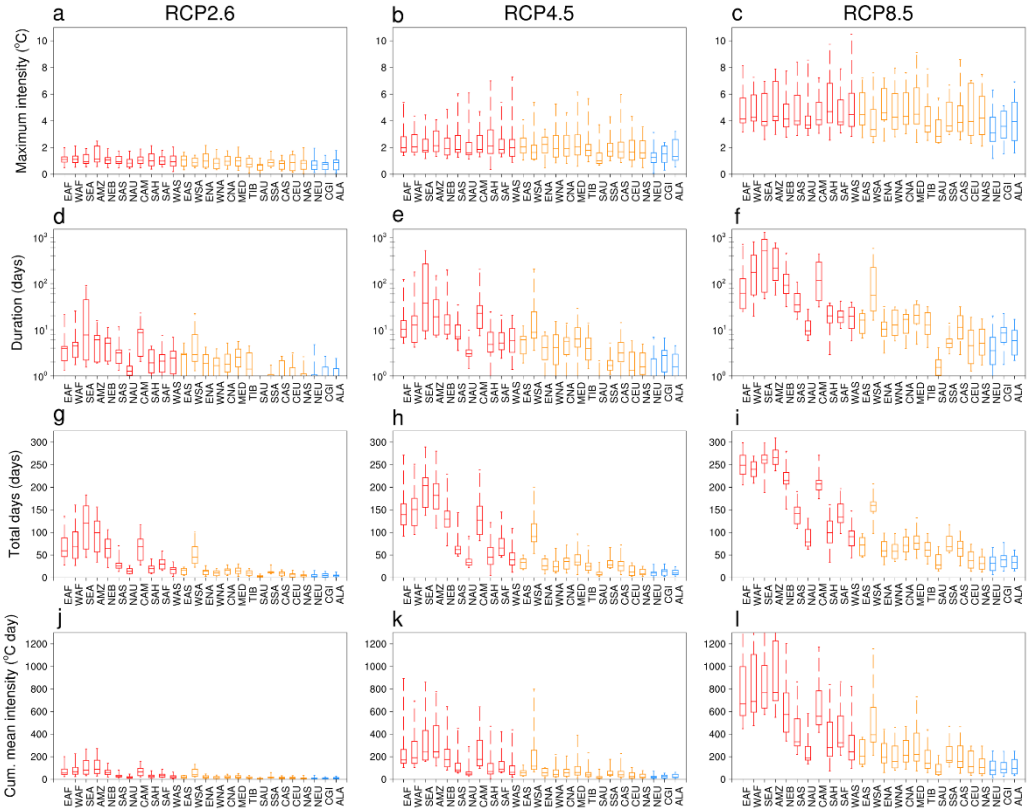


**Figure 5**. Regional changes in HSW characteristics averaged between 2081 and 2100 under RCP2.6, 4.5 and 8.5 relative to the historical 1986-2005 period. Simulated variations in maximum annual intensity (a-c), annual mean duration (d-f), number of total HSW days per year (g-i), and annual cumulative mean intensity (j-l). Note that the logarithmic scale is used in (d-f). Global land areas between 66°S and 66°N are represented by 26 world regions (see Figure S2, Table S2). Based on area-weighted average latitude, these regions are classified into the low (red), mid (orange), and high (blue) latitudes.

In the historical period, the PR medians of HSWs are no more than 10 in all 26 regions (Figure 6a). During 2081-2100, in the tropical regions like EAF, WAF, SEA, AMZ, NEB and CAM, the models project a 60-fold increase (with reference to pre-industrial conditions) in the probability of occurrence of a HSW under RCP 8.5 (Figure 6g). The simulated FAR of these regions can rise to its maximum value 0.99, and thus the multi-model spread is much smaller than other regions (Figure 6h). For most mid and high latitudes, the PR and FAR are expected

to reach the historical level of the tropical regions, following low and middle future emissions (Figure 6a-f).

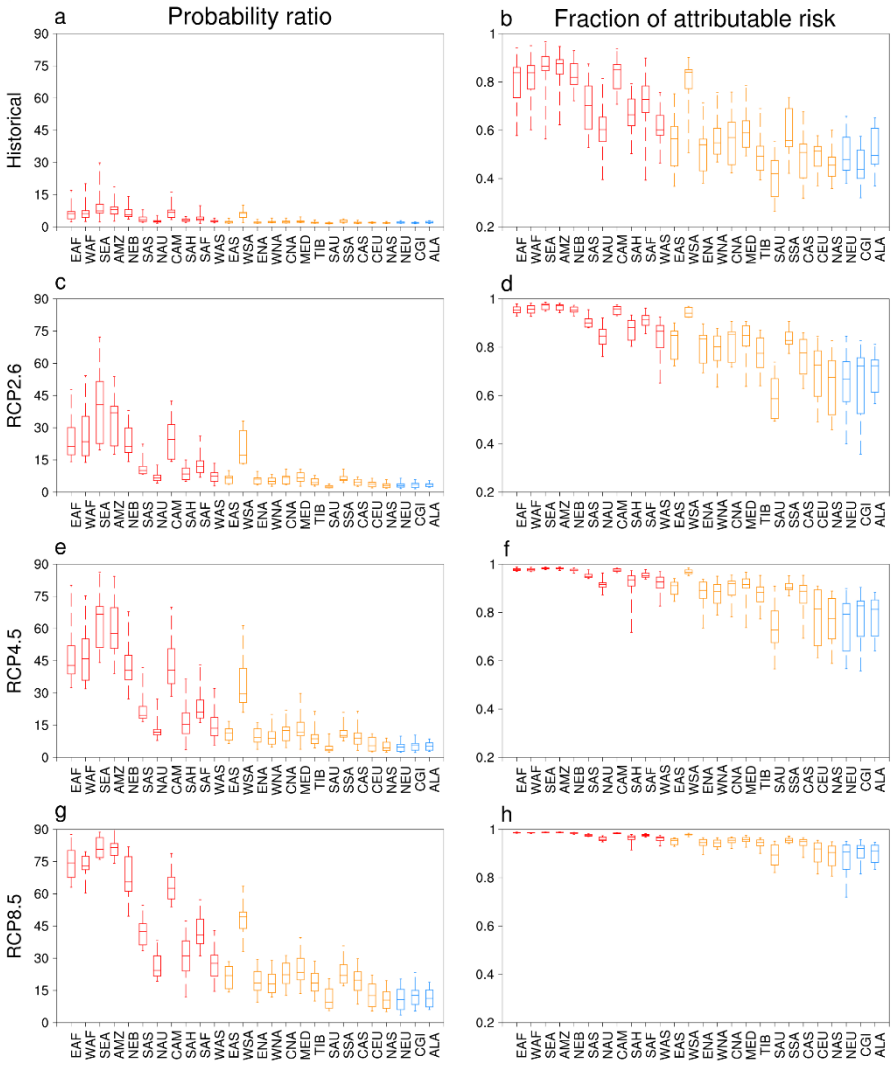


**Figure 6**. Attribution of regional HSWs in the historical and future periods. (a,c,e,g) Probability of HSW days exceeding the preindustrial 99th percentile; (b,d,f,h) anthropogenic contribution to the probability of HSWs. Results are shown for the historical 1986-2005 period and for the 2081-2100 period under all three RCPs. Global land areas between 66°S and 66°N are represented by 26 world regions (see Figure S1, Table S2). Based on area-weighted average latitude, these regions are classified into the low (red), mid (orange), and high (blue) latitudes.

### 3.3 Regional population exposure to HSWs

Research has identified that continued climate change could lead to hundreds of millions more people regularly exposed to deadly heat (Coffel et al., 2018; Im et al. 2017; Matthews et al., 2017; Mora et al., 2017). We here present the analysis of population exposed to HSWs for 26 world regions, combining with regional vulnerability to heat stress extremes. The disparities in the number of HSW days and population lead to a wide spread of regional population exposure to HSWs (Figure 7). In the historical period, regions which have the largest mean exposure of 8-10 million person-days, such as South Asia (SAS) and Southeast Asia (SEA), all have

relatively low GDP per capita (Figure 7a). For most other regions, the exposure is less than 2 million person-days (Figure 7a).

Exposure to HSWs depends heavily on the combination of future GHG emissions and socioeconomic scenarios. However, regardless of which combined scenario is considered, South Asia (SAS), Southeast Asia (SEA), East Africa (EAF), West Africa (WEF), and Central America and Caribbean (CAM) among 26 world regions are projected to experience the largest increase in exposure, relative to the historical level (Figure 7b-g). For instance, even if the world evolves toward a sustainable future via highly mitigated GHG emissions (RCP2.6) and low population growth (SSP1), SAS still expects to see roughly a quadrupling of population exposure on average, from 9 million person-days to 40 million person-days (Figure 7a,b). The scenario combining unmitigated emissions (RCP8.5) and rapidly growing populations (SSP3) is projected to see an over thirtyfold increase to around 300 million person-days (Figure 7a,f). For most other regions, our results suggest the increase in annual mean exposure to be less than 5, 20 and 40 million person-days under RCP2.6-SSP1, RCP4.5-SSP2 and RCP8.5-SSP3, respectively (Figure 7c,e,g).

In the worst climatic and socioeconomic projection (RCP8.5 and SSP3), regions witnessing the largest increase in population exposure are also anticipated to have the slowest economy growth (that is, SAS, SEA, EAF, WAF and CAM; Figure 7f,g). It implies that people in these regions may have the most limited resources to adapt to the potential impact of extreme heat toward the end of century. Note that these regions are all the low latitudes with relatively high mean WGBT; so it is their lives rather than body comfort that could be seriously threatened (Mora et al., 2017). For the moderately extreme projection (RCP4.5 and SSP2), GDP per capita increase of SEA and CAM is expected to be a medium level, but EAF, WAF and SAS may still be the worst economically developed (Figure 7d,e). Whereas in the most sustainable future projection (RCP2.6 and SSP1), we project that population of all these five regions are not the poorest anymore, and SEA and CAM could even become rather wealthier socio-economic places (Figure 7b,c).

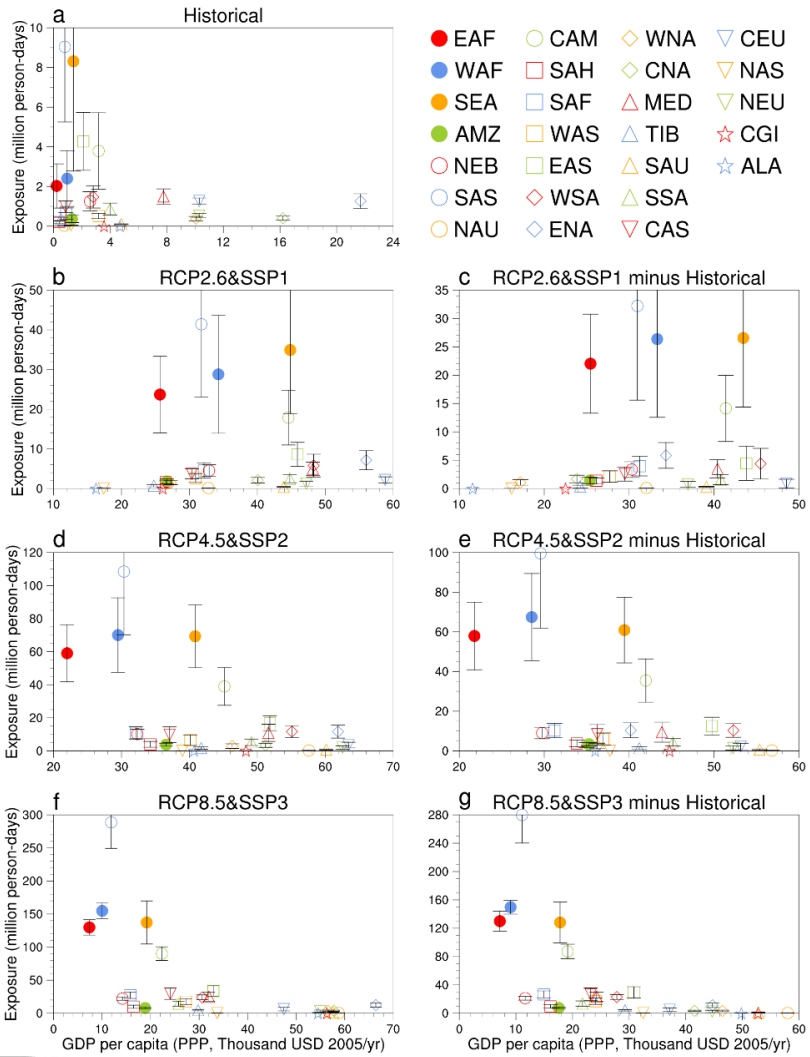


**Figure 7**. Regional mean population exposure to HSWs. Regional mean annual exposure to HSWs and GDP per capita in the historical 1986-2005 period (a) and the 2081-2100 period under RCP2.6-SSP1 (b), RCP4.5-SSP2 (d) and RCP8.5-SSP3 (f). Changes in exposure and GDP per capita during 2081-2100 for three scenarios relative to 1986-2005 (c,e,g). Regional division is the same as given in Figure S2 and Table S2.

### 3.4 Changes in HSWs with GMST increasing

Perkins-Kirkpatrick and Gibson (2017) investigated how different regional heatwave characteristics (intensity, frequency and duration) are projected to change relative to increasing global warming thresholds. Until now, we have not known how multiple characteristics of heat stress extremes will change with respect to global temperature increasing. Here, we evaluate the projected changes in HSWs under all three emissions scenarios as a function of global mean surface temperature (GMST). Results are also considered globally (Figure 8) and for 26 land-based regions (Figures S3-S7). The magnitude of changes in HSW characteristics scales with the GMST and this scaling is independent of forcing pathway, it refers to amounts of GMST (Figure 8 and Figures S3-S7). This is similar to the results of Matthews et al. (2017) showing that the potential societal consequences from increasing humid heat count on amounts of climate warming rather than RCPs.

On both global and regional scales, changes in the maximum intensity are linear with respect to GMST increasing, and the intensity is projected to increase by approximately the same amount as GMST (Figure 8a and Figures S3-S7). However, there is not a clear linear relationship between the other three characteristics and GMST (Figure 8c-d and Figures S3-S7). Most regions see a sharper increase in the mean duration and cumulative mean intensity from 15-16 °C, suggesting that the length of HSWs are more sensitive to higher increases in global temperature. Note that the uncertainty of duration projection becomes large at the warm tail, especially for some tropical regions where longer consecutive days are expected. Regions with larger overall increases in the annual total HSW days display slower rates of change above 16 °C, as the maximum number of HSW days in a year is approached (such as EAF, WAF, SEA, AMZ, NEB CAM and WSA). In contrast, over the other regions, changes in the HSW days are nearly linear.

Furthermore, the global and regional coefficients of HSW changes relative to per degree of GMST increasing are quantified. Given that over most regions, the three characteristics (duration, annual total HSW days and cumulative mean intensity) projected by CMIP5 change at a non-linear rate, the slopes of linear fitting lines are considered as the average rates of increase (Figure 8, Figures S3-S7 and Table 1). Globally-averaged maximum intensity, mean duration, total HSW days and cumulative mean intensity is projected to increase by approximately 0.94 °C, 6.8 days, 20 days and 76.29 °C days per degree of GMST increasing, respectively (Figure 8). Over all 26 regions, the maximum intensity is projected to increase approximately 1:1 with GMST (Table 1). The largest and smallest increase occurs over Eastern North America (ENA), and South Australia and New Zealand (SAU), where the intensity is projected to increase by 1.09 °C and 0.71 °C per °C GMST increasing, respectively. For the other three characteristics, there is large regional variation in the rates of their changes, and more rapid increases generally occur over tropical regions (Table 1). The multi-model mean change in the duration is mostly between 1 and 5 days. Larger increases of approximately 10-20 days occur in East and West Africa (EAF and WAF), Northeast Brazil (NEB), Central America and Caribbean (CAM), and West coast of South America (WSA), per °C of GMST rise. Southeast Asia (SEA) and Amazon (AMZ) are projected to have the largest rate of increase, with 32 days and 29 days, respectively. The annual total HSW days and cumulative mean intensity also show the most striking changes in some tropical regions, with around 40 days and over 100 °C days over EAF, WAF, SEA, AMZ, NEB and CAM, per degree of GMST increasing. The increase in the duration and intensity leads to a strongest increase in the cumulative mean intensity of 212 °C days in AMZ. These changes are less severe in the mid to high latitudes, where about 7-20 days and 20-60 °C days are expected across Northern America, Europe and Russia.

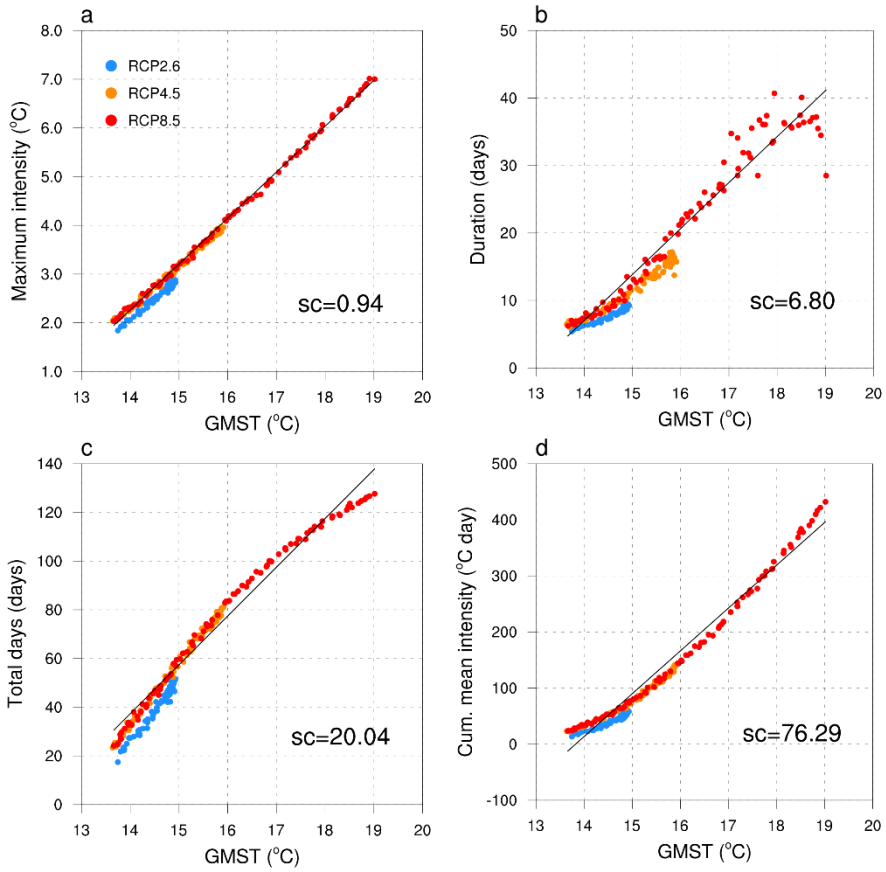


**Figure 8**. Global average changes in HSWs relative to GMST for annual maximum intensity (a), annual mean duration (b), annual total HSW days (c) and annual cumulative mean intensity (d). Results derive from the future simulation (2006-2100) under all three emissions scenarios. Linear fitting line (black line) and its slope coefficient (sc) are also shown in each panel.

**Table 1.** *Multi-model mean regional coefficients of HSW changes relative to per degree of global mean surface temperature (GMST) increasing*

| Region | Maximum intensity | Mean duration | HSW days | Cumulative intensity |
|---|---|---|---|---|
| EAF | 0.94 | 14.96 | 47.45 | 172.66 |
| WAF | 0.98 | 20.44 | 44.95 | 179.79 |
| SEA | 0.96 | 31.80 | 41.02 | 173.61 |
| AMZ | 1.08 | 28.96 | 48.58 | 211.98 |
| NEB | 0.92 | 12.96 | 40.66 | 141.23 |
| SAS | 0.96 | 7.86 | 28.27 | 92.11 |
| NAU | 0.85 | 2.13 | 17.69 | 55.41 |
| CAM | 0.92 | 15.01 | 37.00 | 139.20 |
| SAH | 1.06 | 4.58 | 19.85 | 78.13 |
| SAF | 0.91 | 4.58 | 28.19 | 96.11 |
| WAS | 1.00 | 4.56 | 17.70 | 66.55 |
| EAS | 1.02 | 3.33 | 14.58 | 51.93 |
| WSA | 0.78 | 12.09 | 25.49 | 95.37 |
| ENA | 1.09 | 2.69 | 13.43 | 51.46 |
| WNA | 0.96 | 3.49 | 12.72 | 44.55 |
| CNA | 1.01 | 3.42 | 15.08 | 54.28 |
| MED | 1.02 | 4.72 | 15.88 | 60.60 |
| TIB | 0.84 | 3.38 | 12.88 | 39.61 |
| SAU | 0.71 | 0.40 | 7.48 | 20.26 |
| SSA | 0.87 | 1.22 | 15.92 | 51.69 |
| CAS | 0.89 | 2.98 | 13.46 | 42.75 |
| CEU | 0.94 | 1.47 | 8.94 | 32.02 |
| NAS | 0.95 | 1.46 | 7.32 | 27.80 |
| NEU | 0.74 | 1.35 | 7.38 | 22.89 |
| CGI | 0.73 | 2.05 | 8.54 | 24.17 |
| ALA | 0.86 | 1.57 | 7.73 | 25.75 |

## 4 Conclusions and Discussion

A novel aspect of this study involves investigating spatial-temporal changes in multiple HSW characteristics (maximum intensity, duration, number of HSW days and cumulative mean intensity) under low, moderate, and high emissions scenarios. In addition, for the first time, the present study demonstrates the varying and concerning rates HSWs over many regions are projected to change, relative to global mean surface air temperature. We think it is an essential addition to the existing literature. Matthews (2018) proposed that there is a need to quantify changes to the intensity (rather than just the frequency) of heat extremes under sustained climate warming. Besides, it is not only the frequency of threshold exceedances, but also the other distinctive characteristics of HSWs that result in the vast array of adverse impacts. For instance, excessive human morbidity or mortality are clearly associated with sustained extreme heat stress (Basu & Samet, 2002).

On average over global land regions, large differences in multiple HSW characteristics are projected during the 21st century under different emissions scenarios, and all features show the most striking increases following a high future emission (RCP 8.5). By 2100, the multi-model ensemble suggests an average increase in the number of HSW days in a year and annual cumulative mean intensity by a factor of 4 and 13 under RCP8.5, relative to the present-day level (that is, the beginning of simulation period). Besides, it projects that the increase in the annual maximum intensity and mean duration can reach 4 °C and 28 days. A one-in-a-hundred-days HSW at preindustrial levels is projected to become a one-in-fifteen-days event in the present climate, and a one-in-nine-days, one-in-five-days and one-in-three-days event forced with RCP 2.6, 4.5 and 8.5 for the late 21st century. Correspondingly, the simulated FAR suggests that roughly 58%, 70%, 80% and 90% of the HSWs worldwide can be attributable to global warming.

Many previous studies have indicated that it is the tropics and subtropics that will generally witness the largest increases in the frequency of extreme values in heat stress indices (Matthews et al., 2017; Mora et al., 2017; Willet & Sherwood, 2012; Zhao et al., 2015). This study also suggests that the duration and cumulative mean intensity exhibit zonal differences, increasing from mid-latitudes to the tropics. The exception is the maximum intensity, showing a relative uniform increase over most of global land. For the increase in probability of HSWs and FAR, it differs across regions and is most pronounced over the tropics. This trend can be understood as being a result of the climatological distribution of WBGT (Figure S8). The weak seasonal cycle and low interannual temperature variability in the tropics (Deser et al., 2012) result in a narrower WBGT spread compared to that in the higher latitudes, and there is a much higher proportion of time in a year spent crossing the HSW threshold (Figure S8). Therefore, even a small increase in the mean can cause a relatively large increase in the frequency of threshold exceedances (Matthews, 2018; Mora et al., 2017; Willett & Sherwood, 2012).

Different than dry heat waves, moist heat stress may occur over large regions for months at a time including densely populated regions in a warmer world (Buzan & Huber, 2020). We project that among 26 world regions, South and Southeast Asia, East and West Africa, and Central America will experience the largest increase in mean population exposure to HSWs by 2100. These regions are also expected to be the least economically developed under RCP8.5-SSP3, thus people there may unable to take enough social adaptions to minimize the potential impacts of HSWs. For example, while air conditioning is a crucial form of adaptation to extreme heat, it is often inaccessible in lower income areas (Carleton et al., 2018). Besides, air conditioning will become useless if there is a power failure, and it may decrease humans' natural thermal adaptability (Matthews et al., 2019). By contrast, in the moderately extreme projection (RCP4.5 and SSP2) and most sustainable projection (RCP2.6 and SSP1), risk of extreme heat may be reduced due to improved socio-economic conditions. Results emphasize the importance of aggressive mitigation.

A recent study has indicated that the frequency of heat-humidity extremes is strongly related to global mean surface air temperature and nearly independent of forcing pathway (Li et al., 2020). We think the present study is an essential addition to the literature. Because our results also confirm changes in other extreme heat characteristics (maximum intensity, duration and cumulative mean intensity) rather than the frequency, independent of emissions scenarios,

referring to amounts of GMST. An approximately 1:1 increase in the maximum intensity relative to GMST occurs over all 26 regions. However, for the other three characteristics, they present very large regional variation, and generally increase more rapidly over the lower latitudes. Multi-model ensemble suggests that the regional increases in the annual mean duration, annual total HSW days and annual cumulative mean intensity can vary largely from about 1 day to 30 days, from 7 days to 49 days, and from 20 °C days to over 200 °C days, per °C of GMST increasing, respectively. Although Matthews et al. (2017) has confirmed that GMST is nonlinearly related to frequency of extreme values in heat stress indices at global scale, our results highlight the different trajectories at which multiple HSW characteristics are projected to change relative to GMST rise. Besides the highly linear increase in annual maximum intensity, the nonlinear changes in annual mean duration and cumulative mean intensity as a function of GMST are also demonstrated, on both global and regional scales. For the number of regional HSW days change, it is projected to be nearly linear in most regions.

Previous study suggested that model biases in simulating temperature over 26 regions have a negligible effect on the projected regional change in heat waves (Giorgi & Coppola, 2010). In the present study, the CMIP5 models really display some biases in simulating the magnitude of HSW characteristics, but the biases are relatively small compared to the future changes. By applying the multi-model ensemble mean that is crucial to study the response of heat stress to climate change (Zhao et al., 2015), the model errors can be reduced to some extent. By using percentile thresholds that are defined from pre-industrial control runs, no assumption is made regarding the underlying probability distribution of WBGT, and the problem of observational uncertainty can be avoided. Note that the biases in higher-order moments such as variance or skewness are not considered, because a bias correction of them with observational data will potentially induce a high uncertainty (Fischer & Knutti, 2015). Given that different systematic biases can lead to opposing corrections, and given that it is difficult to identify all manifestations of all biases, it follows that the most appropriate way to improve climate projections is to keep working toward more realistic climate models (Wang et al., 2017). This is far beyond the scope of this study.

Utilizing simple and usually empirically based heat stress indicators is a common practice in meteorological and climate projection of heat stress related human mortality and morbidity (Buzan & Huber, 2020; Matthews, 2018). Numerous heat stress indices have been developed, varying widely in their level of complexity, input parameters, parameter weightings, physiological assumptions, etc (Willet & Sherwood, 2012). The present study only uses one of them to evaluate heat extremes, and neglects the effects of wind and solar insolation. Although the underlying moist thermodynamic theory is the same, the pattern analysis of Buzan and Huber (2020) highlights the importance of using multiple heat stress metrics to capture the diversity of potential impacts. In addition, we only quantify future regional population exposure to HSWs under three combined RCP and SSP scenarios. In particular, Gidden et al. (2019) presented the key deliverable of the ScenarioMIP experiment within CMIP6, which involves nine scenarios of future emissions trajectories of anthropogenic sources. Future work could endeavor to evaluate exposure and vulnerability to extreme heat under more climatic and socioeconomic scenarios for use in CMIP6.

**Acknowledgments**

We thank the Data Distribution Centre of the Intergovernmental Panel on Climate Change for making the CMIP5 multi-model datasets available (http://www.ipcc-data.org/sim/gcm_monthly/AR5/Reference-Archive.html). We acknowledge the European Centre for Medium-Range Weather Forecasts for their reanalysis data (https://climate.copernicus.eu/climate-reanalysis). We also thank Drs. Murakami and Yamagata for the downscaled population and GDP data from the SSPs (http://www.cger.nies.go.jp/gcp/population-and-gdp.html). This work was supported by funding from the National Key Research and Development Program of China (Grant 2016YFA0602403), National Natural Science Foundation of China (Grant 41775103 and 41907395), Second Tibetan Plateau Scientific Expedition and Research Program (Grant 2019QZKK0906 and 2019QZKK0606).

**References**

Australian Bureau of Meteorology (ABOM). (2010). http://www.bom.gov.au/info/thermal_stress/

Alexander, L. V., et al. (2006). Global observed changes in daily climate extremes of temperature and precipitation. *Journal of Geophysical Research: Atmospheres*, *111*(D5). https://doi.org/10.1029/2005jd006290

Angélil, O., Stone, D. A., & Pall, P. (2014). Attributing the probability of South African weather extremes to anthropogenic greenhouse gas emissions: Spatial characteristics. *Geophysical Research Letters*, *41*(9), 3238-3243. https://doi.org/10.1002/2014GL059760

Barriopedro, D., Fischer, E. M., Luterbacher, J., Trigo, R. M., & García-Herrera, R. (2011). The Hot Summer of 2010: Redrawing the Temperature Record Map of Europe. *Science*, *332*(6026), 220-224. https://doi.org/10.1126/science.1201224

Basu, R., & Samet, J. M. (2002). Relation between Elevated Ambient Temperature and Mortality: A Review of the Epidemiologic Evidence. *Epidemiologic Reviews*, *24*(2), 190-202. https://doi.org/10.1093/epirev/mxf007

Buzan, J. R., & Huber, M. (2020). Moist Heat Stress on a Hotter Earth. *Annual Review of Earth and Planetary Sciences*, *48*(1), 623-655. https://doi.org/10.1146/annurev-earth-053018-060100

Buzan, J. R., Oleson, K., & Huber, M. (2015). Implementation and comparison of a suite of heat stress metrics within the Community Land Model version 4.5. *Geoscientific Model Development*, *8*(2), 151-170. https://doi.org/10.5194/gmd-8-151-2015

Carleton, T., et al. (2018). Valuing the Global Mortality Consequences of Climate Change Accounting for Adaptation Costs and Benefits. *SSRN Electronic Journal*. https://doi.org/10.2139/ssrn.3224365

Chen, X., Li, N., Liu, J., Zhang, Z., & Liu, Y. (2019). Global Heat Wave Hazard Considering Humidity Effects during the 21st Century. *International Journal of Environmental Research and Public Health*, *16*(9), 1513.

Coffel, E. D., Horton, R. M., & de Sherbinin, A. (2018). Temperature and humidity based projections of a rapid rise in global heat stress exposure during the 21st century. *Environmental Research Letters*, *13*(1), 014001. https://doi.org/10.1088/1748-9326/aaa00e

Deser, C., Phillips, A., Bourdette, V., & Teng, H. (2012). Uncertainty in climate change projections: the role of internal variability. *Climate Dynamics*, *38*(3), 527-546. https://doi.org/10.1007/s00382-010-0977-x

Dong, W., Liu, Z., Liao, H., Tang, Q., & Li, X. e. (2015). New climate and socio-economic scenarios for assessing global human health challenges due to heat risk. *Climatic Change*, *130*(4), 505-518. https://doi.org/10.1007/s10584-015-1372-8

Dunne, J. P., Stouffer, R. J., & John, J. G. (2013). Reductions in labour capacity from heat stress under climate warming. *Nature Climate Change*, *3*(6), 563-566. https://doi.org/10.1038/nclimate1827

Fischer, E. M., & Knutti, R. (2013). Robust projections of combined humidity and temperature extremes. *Nature Climate Change*, *3*, 126-130. https://doi.org/10.1038/nclimate1682

Fischer, E. M., & Knutti, R. (2015). Anthropogenic contribution to global occurrence of heavy-precipitation and high-temperature extremes. *Nature Climate Change*, *5*, 560-564. https://doi.org/10.1038/nclimate2617

Fischer, E. M., Oleson, K. W., & Lawrence, D. M. (2012). Contrasting urban and rural heat stress responses to climate change. *Geophysical Research Letters*, *39*(3). https://doi.org/10.1029/2011GL050576

Frolicher, T. L., Fischer, E. M., & Gruber, N. (2018). Marine heatwaves under global warming. *Nature*, *560*(7718), 360-364. https://doi.org/10.1038/s41586-018-0383-9

García-Herrera, R., Díaz, J., Trigo, R. M., Luterbacher, J., & Fischer, E. M. (2010). A Review of the European Summer Heat Wave of 2003. *Critical Reviews in Environmental Science and Technology*, *40*(4), 267-306. https://doi.org/10.1080/10643380802238137

Gidden, M. J., et al. (2019). Global emissions pathways under different socioeconomic scenarios for use in CMIP6: a dataset of harmonized emissions trajectories through the end of the century. *Geoscientific Model Development*, *12*(4), 1443-1475. https://doi.org/10.5194/gmd-12-1443-2019

Giorgi, F., & Coppola, E. (2010). Does the model regional bias affect the projected regional climate change? An analysis of global model projections. *Climatic Change*, *100*(3), 787-795. https://doi.org/10.1007/s10584-010-9864-z

Harrington, L. J., Frame, D., King, A. D., & Otto, F. E. L. (2018). How Uneven Are Changes to Impact-Relevant Climate Hazards in a 1.5 °C World and Beyond? *Geophysical Research Letters*, *45*(13), 6672-6680. https://doi.org/10.1029/2018gl078888

Im, E. S., Pal, J. S., & Eltahir, E. A. B. (2017). Deadly heat waves projected in the densely populated agricultural regions of South Asia. *Sci Adv*, *3*(8), e1603322. https://doi.org/10.1126/sciadv.1603322

IPCC. (2012). In C. B. Field, et al. (Eds.), Managing the Risks of Extreme Events and Disasters to Advance Climate Change Adaptation. *A Special Report of Working Groups I and II of the Intergovernmental Panel on Climate Change*. Cambridge, UK and New York, USA: Cambridge University Press.

IPCC. (2014). In Core Writing Team, Pachauri, R. K. & Meyer, L. A. (Eds.), Climate Change 2014: Synthesis Report. *Contribution of Working Groups I, II and III to the Fifth Assessment Report of the Intergovernmental Panel on Climate Change*. IPCC Geneva, Switzerland.

ISO. (1989). Hot Environments—Estimation of the heat stress on working man, based on the

WBGT-index (wet bulb globe temperature), *ISO Standard 7243*. Geneva: International Standards Organization.

Jacobs, S. J., Pezza, A. B., Barras, V., Bye, J., & Vihma, T. (2013). An analysis of the meteorological variables leading to apparent temperature in Australia: Present climate, trends, and global warming simulations. *Global and Planetary Change*, *107*, 145-156. https://doi.org/https://doi.org/10.1016/j.gloplacha.2013.05.009

Jones, B., & O'Neill, B. C. (2016). Spatially explicit global population scenarios consistent with the Shared Socioeconomic Pathways. *Environmental Research Letters*, *11*(8), 084003. https://doi.org/10.1088/1748-9326/11/8/084003

Jones, B., O'Neill, B. C., McDaniel, L., McGinnis, S., Mearns, L. O., & Tebaldi, C. (2015). Future population exposure to US heat extremes. *Nature Climate Change*, *5*(7), 652-655. https://doi.org/10.1038/nclimate2631

Kang, S., & Eltahir, E. A. B. (2018). North China Plain threatened by deadly heatwaves due to climate change and irrigation. *Nature Communications*, *9*(1), 2894. https://doi.org/10.1038/s41467-018-05252-y

King, A. D., & Harrington, L. J. (2018). The Inequality of Climate Change From 1.5 to 2°C of Global Warming. *Geophysical Research Letters*, *45*(10), 5030-5033. https://doi.org/10.1029/2018GL078430

King, A. D., Black, M. T., Min, S. K., Fischer, E. M., Mitchell, D. M., Harrington, L. J., & Perkins-Kirkpatrick, S. E. (2016). Emergence of heat extremes attributable to anthropogenic influences. *Geophysical Research Letters*, *43*(7), 3438-3443. https://doi.org/10.1002/2015gl067448

Knutson, T. R., & Ploshay, J. J. (2016). Detection of anthropogenic influence on a summertime heat stress index. *Climatic Change*, *138*(1-2), 25-39. https://doi.org/10.1007/s10584-016-1708-z

Kovats, R. S. & Hajat, S. (2008). Heat stress and public health: a critical review. *Annual Review of Public Health*, *29*, 41-55. https://doi.org/10.1146/annurev.publhealth.29.020907.090843

Larcom, S., She, P.-W., & van Gevelt, T. (2019). The UK summer heatwave of 2018 and public concern over energy security. *Nature Climate Change*, *9*(5), 370-373. https://doi.org/10.1038/s41558-019-0460-6

Lee, S.-M., & Min, S.-K. (2018). Heat Stress Changes over East Asia under 1.5° and 2.0°C Global Warming Targets. *Journal of Climate*, *31*(7), 2819-2831. https://doi.org/10.1175/jcli-d-17-0449.1

Lemke, B., & Kjellstrom, T. (2012). Calculating Workplace WBGT from Meteorological Data: A Tool for Climate Change Assessment. *Industrial Health*, *50*(4), 267-278. https://doi.org/10.2486/indhealth.MS1352

Li, D., Yuan, J., & Kopp, R. E. (2020). Escalating global exposure to compound heat-humidity extremes with warming. *Environmental Research Letters*, *15*(6), 064003. https://doi.org/10.1088/1748-9326/ab7d04

Li, C., Zhang, X., Zwiers, F., Fang, Y., & Michalak, A. M. (2017). Recent Very Hot Summers in Northern Hemispheric Land Areas Measured by Wet Bulb Globe Temperature Will Be the Norm Within 20 Years. *Earth's Future*, *5*(12), 1203-1216. https://doi.org/10.1002/2017ef000639

Liu, Z., Anderson, B., Yan, K., Dong, W., Liao, H., & Shi, P. (2017). Global and regional changes in exposure to extreme heat and the relative contributions of climate and population change. *Scientific Reports*, *7*(1), 43909. https://doi.org/10.1038/srep43909

Matthews, T. (2018). Humid heat and climate change. *Progress in Physical Geography: Earth and Environment*, *42*(3), 391-405. https://doi.org/doi: 10.1177/0309133318776490

Matthews, T., Wilby, R. L., & Murphy, C. (2019). An emerging tropical cyclone–deadly heat compound hazard. *Nature Climate Change*, *9*(8), 602-606. https://doi.org/10.1038/s41558-019-0525-6

Matthews, T. K. R., Wilby, R. L., & Murphy, C. (2017). Communicating the deadly consequences of global warming for human heat stress. *Proceedings of the National Academy of Sciences*, *114*(15), 3861. https://doi.org/10.1073/pnas.1617526114

Meehl, G. A., & Tebaldi, C. (2004). More Intense, More Frequent, and Longer Lasting Heat Waves in the 21st Century. *Science*, *305*(5686), 994-997. https://doi.org/10.1126/science.1098704

Mora, C., et al. (2017). Global risk of deadly heat. *Nature Climate Change*, *7*, 501. https://doi.org/10.1038/nclimate3322

Murakami, D., & Yamagata, Y. (2019). Estimation of Gridded Population and GDP Scenarios with Spatially Explicit Statistical Downscaling. *Sustainability*, *11*(7), 2106. https://doi.org/10.3390/su11072106

O'Neill, B. C., Kriegler, E., Riahi, K., Ebi, K. L., Hallegatte, S., Carter, T. R., Mathur, R., & van Vuuren, D. P. (2014). A new scenario framework for climate change research: the concept of shared socioeconomic pathways. *Climatic Change*, *122*(3), 387-400. https://doi.org/10.1007/s10584-013-0905-2

Pal, J. S., & Eltahir, E. A. B. (2015). Future temperature in southwest Asia projected to exceed a threshold for human adaptability. *Nature Climate Change*, *6*(2), 197-200. https://doi.org/10.1038/nclimate2833

Patz, J. A., Campbell-Lendrum, D., Holloway, T., & Foley, J. A. (2005). Impact of regional climate change on human health. *Nature*, *438*(7066), 310-317. https://doi.org/10.1038/nature04188

Perkins-Kirkpatrick, S. E., & Gibson, P. B. (2017). Changes in regional heatwave characteristics as a function of increasing global temperature. *Scientific Reports*, *7*(1), 12256. https://doi.org/10.1038/s41598-017-12520-2

Raymond, C., Matthews, T., & Horton, R. M. (2020). The emergence of heat and humidity too severe for human tolerance. *Science Advances*, *6*(19), eaaw1838. https://doi.org/10.1126/sciadv.aaw1838

Riahi, K., et al. (2017). The Shared Socioeconomic Pathways and their energy, land use, and greenhouse gas emissions implications: An overview. *Global Environmental Change*, *42*, 153-168. https://doi.org/10.1016/j.gloenvcha.2016.05.009

Russo, S., Dosio, A., Graversen, R. G., Sillmann, J., Carrao, H., Dunbar, M. B., Singleton, A., Montagna, P., Barbola, P., & Vogt, J. V. (2014). Magnitude of extreme heat waves in present climate and their projection in a warming world. *Journal of Geophysical Research: Atmospheres*, *119*(22), 12,500-512,512. https://doi.org/10.1002/2014JD022098

Schleussner, C. F., et al. (2016). Differential climate impacts for policy-relevant limits to global warming: the case of 1.5 °C and 2 °C. *Earth System Dynamics*, *7*(2), 327-351.

https://doi.org/10.5194/esd-7-327-2016

Schoof, J. T., Heern, Z. A., Therrell, M. D., & Remo, J. W. F. (2015). Assessing trends in lower tropospheric heat content in the central United States using equivalent temperature. *International Journal of Climatology*, *35*(10), 2828-2836. https://doi.org/10.1002/joc.4175

Sherwood, S. C., & Huber, M. (2010). An adaptability limit to climate change due to heat stress. *Proceedings of the National Academy of Sciences*, *107*(21), 9552-9555. https://doi.org/10.1073/pnas.0913352107

Stott, P. A., Stone, D. A., & Allen, M. R. (2004). Human contribution to the European heatwave of 2003. *Nature*, *432*(7017), 610-614. https://doi.org/10.1038/nature03089

van Vuuren, D. P., et al. (2011). The representative concentration pathways: an overview. *Climatic Change*, *109*(1), 5. https://doi.org/10.1007/s10584-011-0148-z

Vogel, M. M., Zscheischler, J., Wartenburger, R., Dee, D., & Seneviratne, S. I. (2019). Concurrent 2018 Hot Extremes Across Northern Hemisphere Due to Human-Induced Climate Change. *Earth's Future*, *7*(0). https://doi.org/10.1029/2019ef001189

Wang, G., Cai, W., & Santoso, A. (2017). Assessing the Impact of Model Biases on the Projected Increase in Frequency of Extreme Positive Indian Ocean Dipole Events. *Journal of Climate*, *30*(8), 2757-2767. https://doi.org/10.1175/JCLI-D-16-0509.1

Wang, M., Zhang, D., Adhityan, A., Ng, W. J., Dong, J., & Tan, S. K. (2016). Assessing cost-effectiveness of bioretention on stormwater in response to climate change and urbanization for future scenarios. *Journal of Hydrology*, *543*, 423-432. https://doi.org/https://doi.org/10.1016/j.jhydrol.2016.10.019

Willett, K. M., & Sherwood, S. (2012). Exceedance of heat index thresholds for 15 regions under a warming climate using the wet-bulb globe temperature. *International Journal of Climatology*, *32*(2), 161-177. https://doi.org/10.1002/joc.2257

Yuan, W., et al. (2016). Severe summer heatwave and drought strongly reduced carbon uptake in Southern China. *Scientific Reports*, *6*, 18813. https://doi.org/10.1038/srep18813

Zhao, Y., Ducharne, A., Sultan, B., Braconnot, P., & Vautard, R. (2015). Estimating heat stress from climate-based indicators: present-day biases and future spreads in the CMIP5 global climate model ensemble. *Environmental Research Letters*, *10*(8), 084013. https://doi.org/10.1088/1748-9326/10/8/084013